

Contents lists available at ScienceDirect

#### Journal of the Mechanical Behavior of Biomedical Materials

Journal of het.
Mechanical Behavior of
Biometical Materials

journal homepage: www.elsevier.com/locate/jmbbm



# Effect of osmolarity and displacement rate on cartilage microfracture clusters failure into two regimes

Dipul Chawla a, Melih Eriten a, Corinne R. Henak a,b,c,\*

- <sup>a</sup> Department of Mechanical Engineering, University of Wisconsin-Madison, 1513 University Ave., Madison, WI, 53706, USA
- b Department of Biomedical Engineering, University of Wisconsin-Madison, 1550 University Ave., Madison, WI, 53706, USA
- <sup>c</sup> Department of Orthopedics and Rehabilitation, University of Wisconsin-Madison, 1111 Highland Ave., Madison, WI, 53705, USA

#### ARTICLE INFO

# Keywords: Microindentation Cartilage fracture Osmolarity Contact pressure Strain energy density Clustering Machine learning

#### ABSTRACT

Articular cartilage is a poroviscoelastic (PVE) material with remarkable resistance to fracture and fatigue failure. Cartilage failure mechanisms and material properties that govern failure are incompletely understood. Because cartilage is partially comprised of negatively charged glycosaminoglycans, altering solvent osmolarity can influence PVE relaxations. Therefore, this study aims to use osmolarity as a tool to provide additional data to interpret the role of PVE relaxations and identify cartilage failure regimes. Cartilage fracture was induced using a 100 µm radius spheroconical indenter at controlled displacement rates under three different osmolarity solvents. Secondarily, contact pressure (CP) and strain energy density (SED) were estimated to cluster data into two failure regimes with an expectation maximization algorithm. Critical displacement, critical load, critical time, and critical work to fracture increased with increasing osmolarity at a slow displacement rate whereas no significant effect was observed at a fast displacement rate. Clustering provided two distinct failure regimes, with regime (I) at lower normalized thickness (contact radius divided by sample thickness), and regime (II) at higher normalized thickness. Varied CP and SED in regime (I) suggest that failure in the regime is strain-governed. Constant CP and SED in regime (II) suggests that failure in the regime is dominantly governed by stress. These regimes can be interpreted as ductile versus brittle, or using a pressurized fragmentation interpretation. These findings demonstrated fundamental failure properties and postulate failure regimes for articular cartilage.

#### 1. Introduction

Articular cartilage is an energy dissipative biological material that has impressive resistance to fracture and fatigue. Despite this resistance to damage, when damage occurs it often precedes into degenerative diseases including osteoarthritis because cartilage is avascular with low intrinsic regenerative capacity (Kujala et al., 1994; William H. Robinson et al., 2016). Therefore, understanding mechanisms governing cartilage failure has potential application in delaying degenerative cartilage disease and in developing bioinspired materials.

Cartilage is a poroviscoelastic (PVE) material comprised of fluid and solid phases. The solid matrix is primarily made of collagen (15–20% of the wet weight; 90–95% of collagen fibrils are type II) and proteoglycans (PGs) with negatively charged glycosaminoglycan (GAG) side chains (4–7% of the wet weight) (Mak, 1986; Maroudas et al., 1991; Mow et al., 1980, 1992, 1999; Torzilli, 1985). GAGs govern the compressive and poroelastic (PE) behavior of cartilage (Chiravarambath et al., 2009;

Edelsten et al., 2010; Han et al., 2011; Nia et al., 2011; Sampat et al., 2013; Soulhat et al., 1999; Springhetti and Selyutina, 2018). Because GAGs are negatively charged, adjusting the solvent osmolarity can be used to adjust the apparent compressive and PE behavior (Eisenberg and Grodzinsky, 1985; Khalsa and Eisenberg, 1997; Korhonen and Jurvelin, 2010; Lu et al., 2004; Myers et al., 1984; Wachtel and Maroudas, 1998). Prior studies have shown that increased osmolarity decreased stiffness, increased PVE energy dissipation and decreased permeability (Hwang et al., 2022; Lu et al., 2004; Zimmerman et al., 2021). The collagen network governs the tensile behavior, balances GAG-driven swelling forces, and gives rise to intrinsic solid matrix viscoelastic (VE) behavior (Eisenberg and Grodzinsky, 1985; Hardingham et al., 1987; Lakes, 2009; Lawless et al., 2017; Nguyen and Levenston, 2012; Soulhat et al., 1999; Urban et al., 1979). Cumulatively, PVE relaxations govern the rate-dependent energy dissipative properties of cartilage (Huang et al., 2003; Mak, 1986). Because energy dissipation drives resistance to fatigue and fracture, adjusting the PVE energy dissipation by adjusting

<sup>\*</sup> Corresponding author. 3031 Mechanical Engineering Building, 1513 University Ave, Madison, WI, 53706, USA. *E-mail address:* chenak@wisc.edu (C.R. Henak).

loading rate, solid matrix composition, or solvent osmolarity can be used to provide insight into mechanisms governing fracture.

Cartilage failure mechanisms are incompletely understood, although rate-dependent material response and PVE relaxations play an important role in failure. Previous literature evaluating the response of cartilage to a single impact load has shown that cracks oblique or normal to the surface can be induced depending on the impact energy (Jeffrey et al., 1995; Silyn-Roberts and Broom, 1990; Verteramo and Seedhom, 2007) and observations using confocal microscopy demonstrated perpendicular and random fractures on the articular surface (Repo and Finlay, 1977; Torzilli et al., 1999). Energy dissipation and stress rate predict microcracking under low energy impacts, again indicating a role of PVE relaxations (Kaleem et al., 2017). Failure testing done using a Split Hopkinson Pressure Bar set-up demonstrated a bifurcated response based on strain rates, with higher strain rates resulting in lower ultimate strength and a more brittle-like failure response (Tran et al., 2021). Some studies have found that shear-based failure criteria, consistent with ductile failure, predict failure accurately (Atkinson et al., 1998; Henak et al., 2017). Together, these studies have given rise to the suggestion that cartilage exhibits two distinct failure modes as a result of PVE relaxations: ductile under slow displacement rate and brittle under fast displacement rate. The effect of loading rate on crack extension in cyclic or fatigue loading indicates that PVE relaxations are also important in fatigue failure of cartilage (Kaplan et al., 2017; Sadeghi et al., 2015, 2018). Because PVE relaxations govern the rate-dependent response, they likely have an important role in any transitions between failure regimes. Our prior studies have shown that displacement rate alters the work required to nucleate a cartilage crack in a manner that is dependent on GAG concentration, and that this dependence occurs through alterations in PVE relaxations (Han et al., 2019, 2021). Therefore, this study aims to use osmolarity as a tool to provide additional data to interpret the role of PVE relaxations and identify cartilage failure regimes.

Following the rationale from PVE relaxations and influence of solvent concentration, the first objective of this study was to determine the influence of osmolarity on fracture initiation under extremely fast and extremely slow displacement rates. Displacement rates were chosen to create fracture events pre-PVE-relaxation and post-PVE-relaxation. We hypothesized that altering the solvent osmolarity would affect the critical parameters measured at crack nucleation event. The second objective of this study was to estimate distinct cartilage failure regimes thereby altering PVE relaxations, collagen fibril re-arrangement, and change in osmotic pressure due to solvent concentration.

#### 2. Materials and methods

#### 2.1. Sample preparation

Eighty-seven full-thickness cartilage samples from 16 patellae of 5–6 months old porcine (sex unknown and assumed random) were obtained from the local abattoir. The porcine patellae were wrapped in gauze soaked with phosphate-buffered saline (PBS, pH = 7.4) and stored at

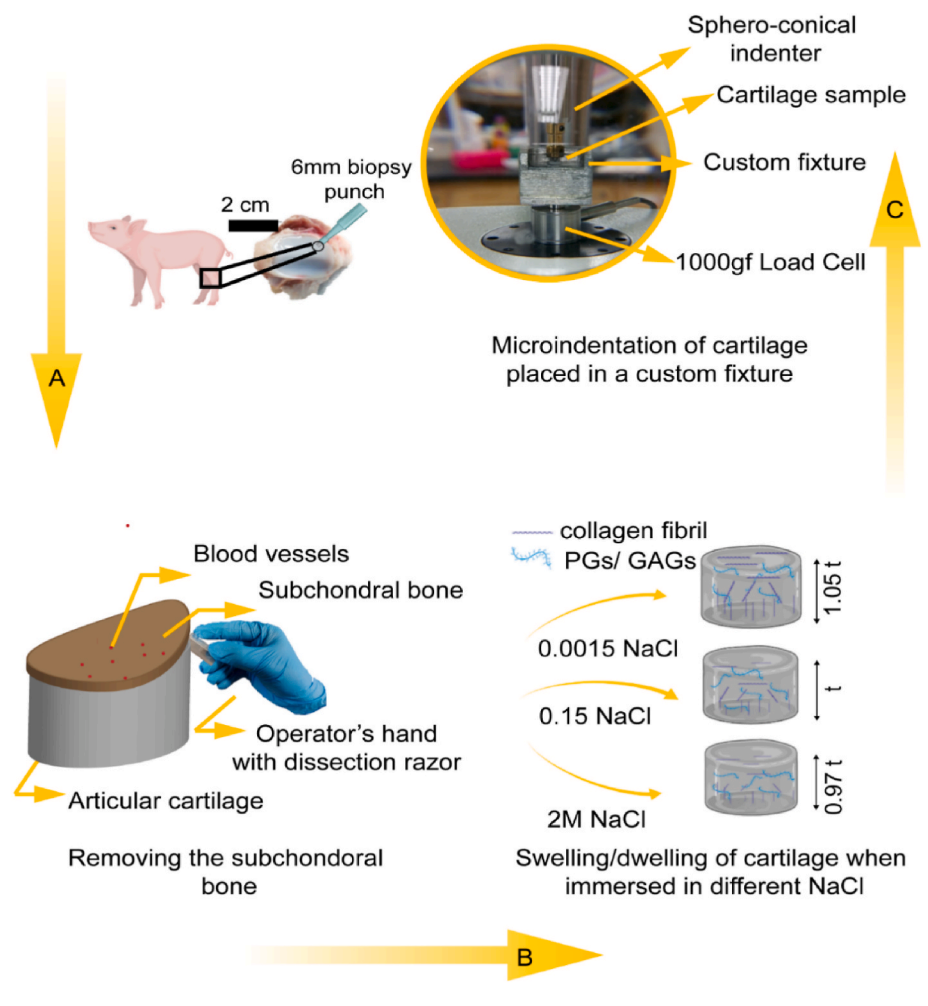


Fig. 1. Schematic illustration of the research methodology: (A) dissection of the porcine patellae and removal of 6 mm cylindrical osteochondral cores, (B) subchondral bone was removed yielding an intact articular cartilage surface and PG/GAGs structural changes leading to swelling/deswelling on immersing it in different concentrations of NaCl; 0.0015 M, 0.15 M, and 2 M, (C) View of the microindentation testing setup used for microfracture.

-20 °C until used for dissection. Samples underwent a single freezethaw cycle prior to testing to minimize changes in the mechanical and material properties (Peters et al., 2017; Qu et al., 2014), best practice is to dissect the sample straight after extraction of the joint surface from the porcine. Cylindrical cores of 6 mm diameter were obtained from each patella using a disposable biopsy punch and scalpel (Fig. 1A). Subchondral bone was removed using a microtome blade and scalpel blades to achieve full thickness cartilage as preferred for mechanical testing (Chawla et al., 2021). Three different osmolarity sodium chloride (NaCl) bathing solutions were made: 0.0015 M NaCl (hypo-osmolarity), 0.15 M NaCl (normal-osmolarity), and 2 M NaCl (hyper-osmolarity). All samples were kept hydrated in NaCl with protease inhibitor (Pierce Mini Tablets, EDTA-free, Thermo Fisher, Waltham, MA) throughout testing. Three groups of 29 cylindrical core samples were immersed in different concentrations of the bathing solutions for 1 h to equilibrate before testing (Fig. 1B). The equilibrium time was selected to achieve constant thickness based on a previous study (Hwang et al., 2022). Sample thickness was measured with digital calipers after equilibration, before samples were placed in testing wells at three to four locations and average cartilage thickness was taken into consideration for this study. The cylindrical core samples were fixed to the custom loading fixture using cyanoacrylate (Loctite 495, Henkel, Germany) and were kept hydrated in their respective bathing solution up to sample's thickness. Average thicknesses were 1.43  $\pm$  0.36 mm, 1.38  $\pm$  0.31 mm, and 1.39  $\pm$  0.25 mm for 0.0015, 0.15, and 2 M NaCl, respectively (Fig. 1B).

#### 2.2. Microfracture experiments

A standard microindentation protocol was used to create microfractures using a diamond sphero-conical indenter with tip radius, R =100  $\mu m$  and tip angle of  $\theta_{\text{tip}}=90^{\circ}$  (Anton Parr, Austria) on tabletop test machine equipped with a 1000 gf load cell (3230-AT series III test Electroforce, TA Instruments, New castle, DE) (Fig. 2A) under displacement control (Chawla et al., 2021). Crack nucleation events were observed by indenting the cartilage samples perpendicular to the articular surface under displacement control test at two extreme displacement rates to capture pre- and post-relaxation regimes: fast displacement rate, FDR (5 mm s $^{-1}$ , n=13 per osmolarity) and slow displacement rate, SDR (0.005 mm s<sup>-1</sup>, n = 16 per osmolarity) (Fig. 2B). These loading rates were selected based on prior research that demonstrated them to cause fracture before and after the majority of poroviscoelastic relaxations occur (Han et al., 2019, 2021). Tests were completed using a ramp waveform up to 35% of the sample thickness in FDR and 80% of the sample thickness in SDR. Critical total work, Wc, critical load,  $L_c$ , critical displacement,  $D_c$ , and critical time,  $T_c$ , were evaluated at the point of major crack nucleation, which was identified as the first decrease in load of more than 30 mN in the load (Fig. 2B). As the

critical times,  $T_{\rm c}$  under FDR are of the order of milliseconds, single crack nucleation point was identified using a high sampling frequency (1707 Hz, 2048 data points per 1.2 s).  $W_{\rm c}$  was calculated as the area under the load-displacement curve from zero to major crack nucleation point using trapezoidal integration in Origin (2019) (OriginLab, MA).

#### 2.3. Microindentation tests at intermediate displacement rates

 $W_{\rm c},~L_{\rm c},~{\rm and}~D_{\rm c}$  data for forty cylindrical samples from a previous study were included in the clustering analysis (Han et al., 2021). Four groups of 10 samples each were hydrated at normal-osmolarity concentration and subjected to microindentation with same sphero-conical indenter of radius,  $R=100~{\rm \mu m}$  and tip angle of  $\theta_{tip}=90^{\circ}$  at four different displacement rates: SDR, FDR, and two other intermediate displacement rates of 0.5 mm s $^{-1}$  (IL1) and 0.05 mm s $^{-1}$  (IL2). Samples were tested intact and after GAG depletion using trypsin. GAG-depleted cartilage samples were also tested at all of three displacement rates except SDR.

#### 2.4. Strain energy density, contact pressure, and failure regime clustering

Microindentation of the materials led to localized strains, built-up strain-energy, and localized fluid pressurization near the indenter tip and these are expected to influence the material response under different loading and environmental conditions.

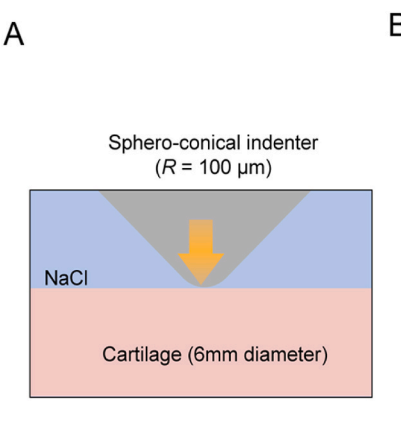
CP and SED were calculated to evaluate different failure regimes (Shergold and Fleck, 2005). First, the contact radius, a was determined for a sphero-conical indenter using published relationships (Briscoe et al., 1994). CP was approximated as the critical load divided by a circular projection of the contact radius (eq. (1)). SED was approximated as the critical work divided by a spherical effected volume under the indentation tip (eq. (2)).

$$CP \approx \frac{L_{\rm c}}{\pi a^2}$$
 (eq. 1)

SED 
$$\approx \frac{W_c}{a^3}$$
 (eq. 2)

here,  $\pi a^2$  is the projected contact area,  $a^3$  is an estimation of the strained volume at the instant of crack nucleation. The normalized thickness  $(a_t)$ , ratio of the contact radius to the sample thickness, was calculated to study the CP and SED independent of sample variation in thickness.

Data were clustered into two regimes (I and II) based on CP versus normalized thickness and based on SED versus normalized thickness. Different unsupervised classification algorithms like k-means, fuzzy c-means, and expectation-maximization were tried to cluster the CP, SED, and normalized thickness ( $a_{t}$ ) data (Dempster et al., 1977; Rodriguez et al., 2019). For this study, a standard expectation maximization (EM)



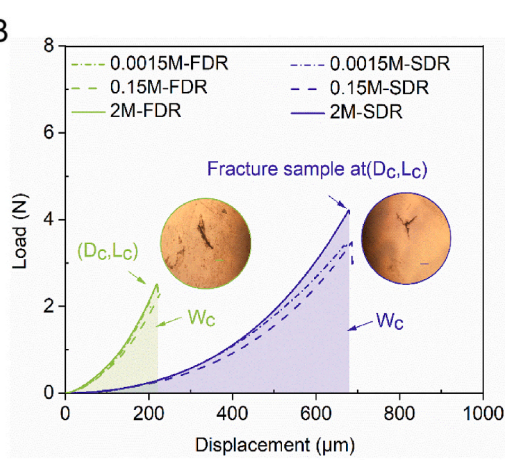


Fig. 2. Microfracture in articular cartilage as a function of two displacement rates and three osmolarity (NaCl) concentration groups: (A) Schematic illustration of the microfracture nucleation testing on cartilage immersed in different concentrations of NaCl with a microscale sphero-conical indenter, (B) Typical load versus displacement curves with critical failure parameters obtained from microfracturing testing with insets of brightfield crack images. under SDR and FDR. Scale bar for insets, 200 µm.

algorithm using a Gaussian mixture models (GMM) was used because it considers "full" and "unshared covariance" which doesn't restrict the shape and size of the cluster with respect to axes and other cluster. The data clustering was done using the Statistics and Machine Learning  $Toolbox^{TM}$  function cluster (MATLAB, 2019a) (additional detail in the Supplementary information).

#### 2.5. Post-test evaluation of fracture morphology

Optical images were used to validate the fracture events induced by microindentation tests at the two displacement rates and three groups of NaCl concentration. India ink was applied on the cracked surface so that it could stain the crack morphology and was gently wiped off. The fractured cartilage surfaces were then imaged using an inverted microscope (IX-71, Olympus, Tokyo, Japan). Tilescan images at  $4 \times$  were used to visualize any additional cracks other than the site of nucleation. In addition to imaging the cracked surfaces, the sphero-conical indenter tip was imaged before and after indenting each sample to confirm that the tip was intact. The tip dimensions, crack lengths, and number of cracks were measured using the segmented line tool ImageJ (version 1.52a, National Institutes of Health).

#### 2.6. Statistical analysis

Differences between response variables (CP, SED,  $W_c$ ,  $L_c$ ,  $D_c$ , and  $T_c$ ) with different NaCl concentration at the two displacement rates were evaluated statistically. The Shapiro test was conducted along with analyzing QQ-plot and histograms to confirm the normality of the dependent variables for each displacement rate and osmolarity. Oneway ANOVAs were used to determine the dependence of CP, SED,  $W_c$ ,  $L_c$ ,  $D_c$ , and  $T_c$  on osmolarity for each displacement rate. At FDR,  $W_c$  and  $L_c$  response variables were not normally distributed, so standard logarithmic transformations were performed to attempt to achieve normality. CP and SED at both displacement rates were not normally distributed and could not be transformed to achieve normality using standard transformations. Therefore, CP and SED were analyzed using a

non-parametric ANOVA. Post-hoc pairwise comparisons were made using Tukey's test. Significance was set at  $p \leq 0.05$ , and 0.05 indicated a trend. All statistical analysis was done using R programming on RStudio® Version 4.0.0 (RStudio, PBC, Boston, MA).

#### 3. Results

### 3.1. Micro-crack nucleation as a function of displacement rate and osmolarity

The influence of the two extreme displacement rates: SDR (0.005 mm s<sup>-1</sup>) and FDR (5 mm s<sup>-1</sup>), and three groups of NaCl concentration: 0.0015 M, 0.15 M, and 2 M, were investigated by nucleating a crack on the surface of the articular cartilage via microindentation. To understand the dependence of the displacement rates and NaCl concentration. the critical failure parameters: critical displacement,  $D_c$ , critical load,  $L_c$ , critical time,  $T_c$ , and critical work,  $W_c$  were evaluated. At SDR, the effect of osmolarity on critical displacement,  $D_c$ , critical load,  $L_c$ , and critical time,  $T_c$ , showed significant difference ( $p \le 0.05$ ) whereas the critical work,  $W_c$ , trended towards significance (0.05 <  $p \le 0.10$ ) (Fig. 3A–D). At SDR, the critical parameters increased with increasing osmolarity. Critical displacement,  $D_c$ , increased by 18.8% from 609.79  $\pm$  150.74  $\mu m$ at 0.0015 M NaCl concentration to 724.37  $\pm$  123.86  $\mu m$  at 2 M NaCl concentration (Fig. 3A). The critical load,  $L_c$ , varied from 3.81  $\pm$  1.74 N at 0.0015 M NaCl concentration to 5.47  $\pm$  1.86 N at 2 M NaCl concentration (Fig. 3B). Critical time,  $T_{\rm c}$ , increased by 19.4% from 118.29  $\pm$ 26.16 s at 0.0015 M NaCl concentration to 141.20  $\pm$  26.15 s at 2 M NaCl concentration (Fig. 3C). Critical work,  $W_c$ , increased by 50% from 0.79  $\pm$  0.42 mJ at 0.0015 M NaCl concentration to 1.18  $\pm$  0.53 mJ at 2 M NaCl concentration (Fig. 3D). At FDR, the critical parameters did not have any significant trend with increasing osmolarity. Critical displacement,  $D_{\rm c}$ , increased by approximately 5% from 211.16  $\pm$  38.70  $\mu m$  at 0.0015 M NaCl concentration to 222.76  $\pm$  44.63  $\mu m$  at 2 M NaCl concentration (Fig. 3A). Critical load,  $\textit{L}_{c}$ , varied from 2.56  $\pm$  0.73 N at 0.0015 M NaCl concentration to 2.99  $\pm$  0.88 N at 2 M NaCl concentration (Fig. 3B). Critical time,  $T_{\rm c}$ , varied from 42.23  $\pm$  7.74 ms at

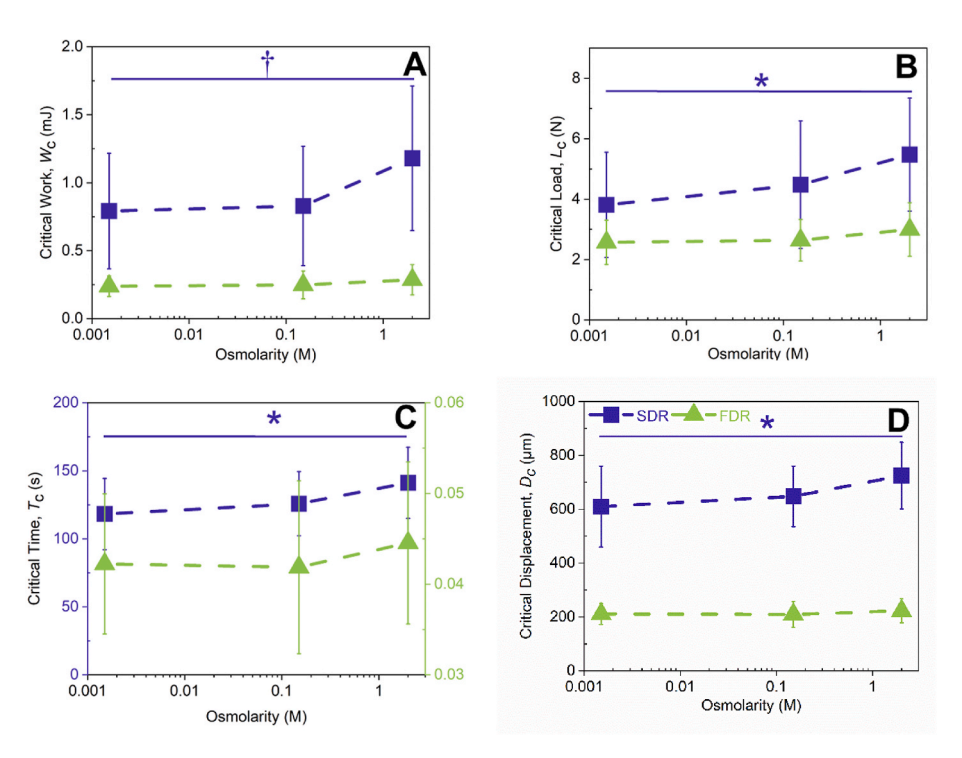


Fig. 3. Experimental results showing critical parameters analyzed during crack nucleation testing: (A) Critical work,  $W_c$  showed an increasing trend with increase in osmolarity at SDR. (B) critical load,  $L_c$ , (C) critical time,  $T_c$ , and (D) critical displacement,  $D_c$ , were all significantly affected by change in osmolarity at SDR. Critical parameters were not statistically different between osmolarities under FDR. The data shows mean  $\pm$  standard deviation (n = 13-16), \* = significant,  $\dagger$  = trend.

0.0015 M NaCl concentration to  $44.55\pm8.92$  ms at 2 M NaCl concentration (Fig. 3C). The critical work,  $W_{c}$ , increased by 16% from  $0.24\pm0.08$  mJ at 0.0015 M NaCl concentration to  $0.28\pm0.11$  mJ at 2 M NaCl concentration (Fig. 3D). No statistical difference was observed in any of the critical parameters ats FDR (Fig. 3A–D). The exact distribution of data points used for understanding the influence of the osmolarity on the critical parameters is shown using violin-box plots in the supplementary data (Fig. S2). For all the NaCl concentrations, the values of the critical parameters decreased as the displacement rate increased. While not tested statistically, dependence of the displacement rate on the critical parameters were consistent with the findings of previous studies (Han et al., 2019, 2021).

#### 3.2. Estimated contact pressure and strain energy density

CP and SED were not significantly different ( $p \geq 0.05$ ) between different osmolarity groups, however, large differences were noted between displacement rates (not tested statistically). CP at FDR (32.91  $\pm$  11.43 MPa) was 4.68 times the estimated CP at SDR (7.02  $\pm$  2.29 MPa). SED at FDR (61.15  $\pm$  33.03 mJ mm $^{-3}$ ) was 6.20 times the estimated SED at SDR (9.86  $\pm$  4.14 mJ mm $^{-3}$ ). CP at the interface of cartilage top surface and indenter's face was approximately equal for normalosmolarity and hyper-osmolarity concentrations at FDR, however, they were 1.10 and 1.07 times the estimated value at hypo-osmolarity concentration, respectively. SED was approximately equal for hypoosmolarity and hyper-osmolarity concentrations at FDR, however, they were 0.92 and 0.91 times the estimated value at the normalosmolarity concentration, respectively.

#### 3.3. Failure regime clustering

Clustering split both CP versus normalized thickness and SED versus normalized thickness into two failure regimes (Fig. 4A and B). The mean normalized thickness of the two regimes were 0.137 and 0.340 for CP, and 0.126 and 0.319 for SED (Supplementary Table S1). Plotting CP versus SED showed a power law relationship, with regime (II) at lower CP and SED values (Fig. 5).

## 3.4. Crack morphology and branching with displacement rates and osmolarity

The brightfield images of the fractured articular surfaces were obtained at  $4 \times \text{magnification}$  after staining the cracked samples with India ink. We observed a transition in crack morphology between the displacement rates representing pre-to post-relaxation timescale. The crack shape varied from two-branched crack at FDR to three-branched crack at SDR, which is consistent with a previous study (Fig. 6) (Han

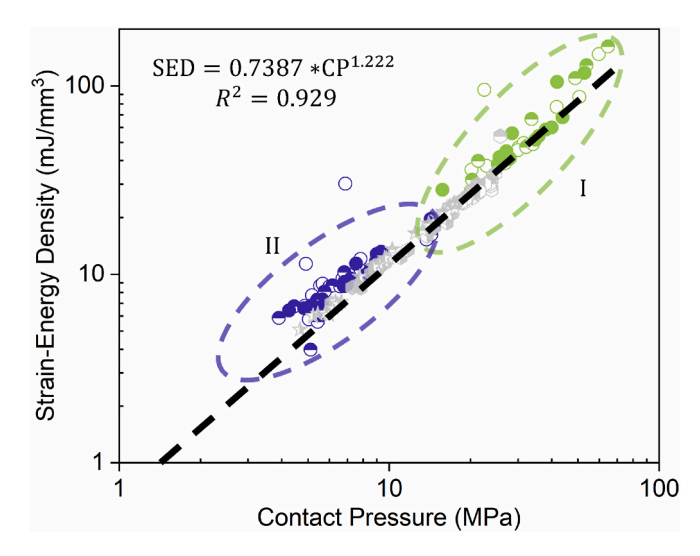


**Fig. 5.** Power law relationship between contact pressure and strain energy density. Regimes I and II are based on the SED clustering.

et al., 2021). At SDR, the crack length varied from 775.46  $\pm$  208.28  $\mu m$  at 0.0015 M NaCl to 764.48  $\pm$  246.84  $\mu m$  at 2 M NaCl concentration. At FDR, the crack length varied from 730.90  $\pm$  149.13  $\mu m$  at 0.0015 M NaCl to 683.76  $\pm$  96.38  $\mu m$  at 2 M NaCl concentration. The crack lengths at normal-osmolarity were 573.61  $\pm$  148.19  $\mu m$  and 759.98  $\pm$  215.56  $\mu m$  at FDR and SDR, respectively, which is consistent with the crack lengths reported in previous study (Han et al., 2021). No consistent trend in the crack morphology, number of branches, or the crack length was observed among samples immersed in hypo-osmolarity, normal-osmolarity, and hyper-osmolarity concentration of the bathing solution at corresponding displacement rates.

#### 4. Discussion

This study examined the effect of osmolarity on cartilage fracture nucleation under extremely fast and extremely slow displacement rates. The data were consistent with the hypothesis that decreased osmolarity decreased critical parameters measured at crack nucleation ( $W_c$ ,  $L_c$ ,  $D_c$ , and  $T_c$ ). The current set of indentation experiments were consistent with our previous studies, which showed a dramatic difference in critical parameters between FDR and SDR, in the pre-PVE-relaxation and post-PVE-relaxation regimes, respectively (Han et al., 2019, 2021). These results are also consistent with prior studies that demonstrate failure at similar nominal stresses (Kaleem et al., 2017), studies that demonstrate rate-dependent failure or tearing (Bartell et al., 2018; Silyn-Roberts and

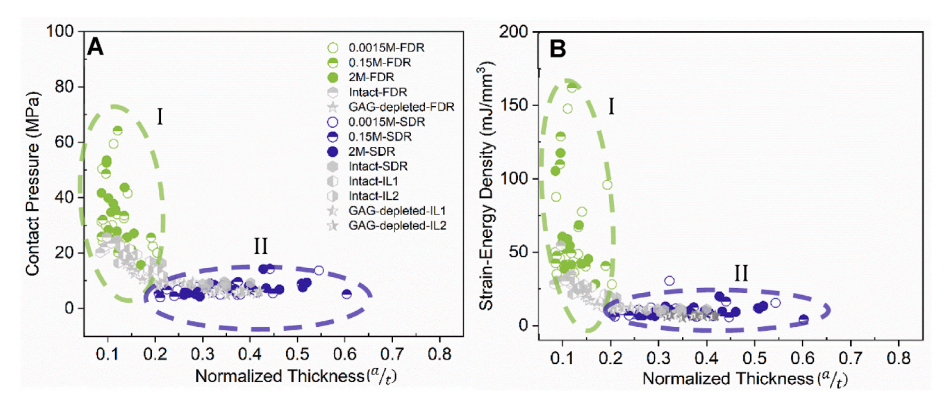
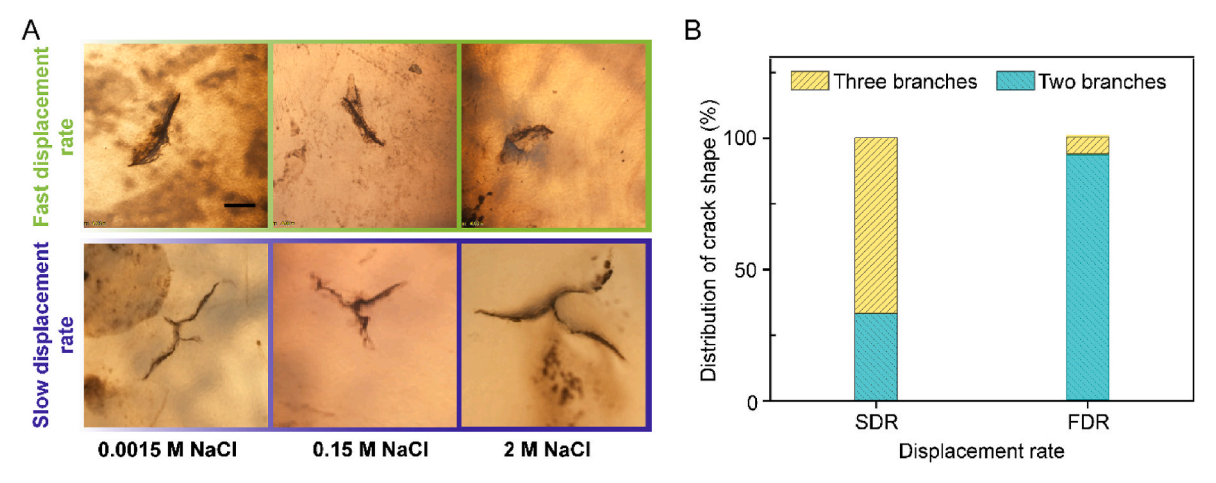


Fig. 4. (A) CP and (B) SED as a function of normalized thickness ( $q_t$ ). CP was estimated by dividing the critical load by the highly stressed contact area beneath the indenter tip. SED was approximated by dividing the critical work required for fracture by the volume envelope in the vicinity of the indenter tip. On the basis of both CP and SED, failure splits into two clusters: regimes (I) and (II) outlined by elliptical sections using EM clustering.



**Fig. 6.** Brightfield images of the fractured cartilage surface: (A) *Top row;* samples tested at fast displacement rate and immersed in increasing order of osmolarity, 0.0015 M through 2 M NaCl, *Bottom row;* samples tested at slow displacement rate and same order of osmolarity, (B) percentage distribution of crack shape for each displacement rate. The morphology changed from two-branched crack to three-branched fractures with an increase in displacement rate. Scale bar, 200 μm.

Broom, 1990), and studies that suggest two distinct failure regimes (Tran et al., 2021). The fast displacement rates are approximately related to activities including jumping, running, kicking, and foot strike (Deneweth et al., 2013; Lieberman et al., 2010; Liu et al., 2010; Nia et al., 2013). The slow displacement rates are approximately related to activities including slow walking or human resting (Cross, 1999; Liu et al., 2010; Long and Srinivasan, 2013; Temple et al., 2016). Decreased critical work with decreased osmolarity is consistent with the findings that decreased osmolarity decreased PVE energy dissipation (Hwang et al., 2022). Thus, the effect of osmolarity on critical parameters at crack nucleation is driven by the altered PVE relaxations with osmolarity. The role of PVE relaxations also explains why osmolarity only influenced critical parameters at SDR. At FDR, loading was too rapid for PVE relaxations to occur (Han et al., 2021), thus removing the effect of osmolarity on critical parameters. The importance of PVE relaxation was corroborated through differences in crack morphology (Fig. 2B insets and Fig. 6), which showed two-branched cracks due to limited re-arrangement of collagen fibers and PVE relaxation at FDR, and three-branched cracks suggesting release of large strain energies in the form of free surfaces at SDR.

Interplay between structural, physical, and mechanical properties of the cartilage solid matrix components changed by immersing the articular cartilage in different concentration NaCl. Changing osmolarity changes permeability, fibril arrangement, and electrostatic charge (Bircher et al., 2020; Levett et al., 2014; Martin-Alarcon and Schmidt, 2016; Myers et al., 1984; Sadeghi et al., 2018; Sampat et al., 2013; Trampel et al., 2002). Decreasing Na+/NaCl concentration (hypoosmolarity) leads to reduced energy dissipation through PVE relaxation and increased thickness because of enhanced electrostatic repulsion between charged PGs and tension in collagen fibrils due to Donnan osmotic pressure (Bircher et al., 2020; Bonifasi-Lista et al., 2005; Chang and Kaplan, 1977; Eisenberg and Grodzinsky, 1985; Hwang et al., 2022; Nguyen and Levenston, 2012; Puxkandl et al., 2002; Tamer, 2013). This decreased PVE relaxation resulted in lower  $L_c$ ,  $W_c$ , and  $D_c$  with decreased osmolarity under SDR. On the contrary, osmolarity did not influence  $L_c$ ,  $W_c$ ,  $D_c$ , or  $T_c$  under FDR. Collagen fibers are under tension at physiological osmolarity of approximately 0.15 M NaCl, and would become more tensed under decreased osmolarity as thickness increases (Maroudas, 1976; Urban et al., 1979). The lack of an osmolarity effect on failure properties under FDR suggests the dominance of PVE-relaxations over collagen fibril tension on failure.

This study grouped failure into two regimes based on CP, SED, and normalized thickness ( $a_t$ ). CP versus normalized thickness ( $a_t$ ) (Fig. 4A) and SED versus normalized thickness ( $a_t$ ) (Fig. 4B) showed a transition

between the regimes (I to II); from lower values of CP and SED at SDR indicating dissipation of energy via fractures with multiple branches (post-PVE-relaxation regime) to higher values of CP and SED at FDR because of localized stresses near the indenter tip (pre-PVE-relaxation regime). In regime (I), CP and SED values varied with normalized thickness, suggesting a regime where failure was governed by strain ( $\alpha / \tau \approx 0.13$ ). Conversely, failure regime (II) had fairly constant CP and SED across a range of normalized thickness values, suggesting a regime where failure was governed by pressure or energy (CP  $\approx$  7 MPa; SED  $\approx$  11 mJ/mm³). Together, these findings suggest a regime (II) where failure is dominantly stress governed, with stress build up as a result of PVE relaxations (Moulinet and Adda-Bedia, 2015).

The existence of two failure regimes could be interpreted in several ways. First, they may indicate brittle failure in regime (I) under FDR and ductile failure in regime (II) under SDR, which would be consistent with prior postulation about cartilage failure mechanisms based on loading rates (Silyn-Roberts and Broom, 1990). However, this possibility is at odds with regime (I) being strain-governed, which would suggest ductile failure (Nalla et al., 2003). Second, they could be interpreted based on localized pressurization. In a highly inflated balloon, puncture results in fragmentation; whereas in a balloon that is minimally inflated, puncture results in a single crack (Moulinet and Adda-Bedia, 2015; Vandenberghe and Villermaux, 2013; Vledouts et al., 2015). Under FDR, displacement was too fast to allow fluid to drain out from the matrix, and would therefore be expected to cause localized fluid pressurization near the vicinity of the indenter tip. Under SDR, the cartilage was squeezed between the indenter tip and the boundary of the test fixture to higher strains giving rise to pressurization along with additional fluid pressurization due to incomplete fluid drainage across the pores. Examining the crack morphology suggests that SDR, with its multiple crack branches, is most consistent with fragmentation failure due to overall pressurization.

While this study provides information suggesting two distinct failure regimes in cartilage, it includes some limitations. This study was designed to understand cartilage failure based on different NaCl concentrations and displacement rates but did not mimic the *in vivo* loading environment. Matching loading based on *in vivo* body weight, and loading rates during day-to-day activities like walking, jumping, and running and osmolarity ranges for healthy, diseased, and degenerated joints is a challenging endeavor (Deneweth et al., 2013; Liu et al., 2010; Mora et al., 2018; William II Robinson et al., 2016). The strains reached, especially in the SDR, were too high to negate the influence of boundary effects; rather, pressurization near the boundary may be governing failure regime II. The current data acquisition coupled with the micro indentation setup can detect major crack nucleation events, especially in

case of extremely fast or traumatic loading rate where the fracture occurs in milliseconds; however there may be smaller drops in load indicating microfracture that this setup was not able to capture. Lastly, while these data suggest two failure regimes, further evidence is needed to identify the governing mechanisms. Future experimental and analytical/computational analyses could further explore the causes of the two regimes, for example by providing evidence of the localized fluid pressurization near the vicinity of the indenter tip hypothesized in regime (f).

In conclusion, this study investigated the effect of solvent osmolarity and displacement rate on the crack nucleation properties and the different failure regimes of the articular cartilage. Tailoring the solvent osmolarity leads to swelling or shrinkage of the cartilage due to osmotic pressure and electrostatic charges caused by GAGs, further inducing changes in mechanical responses like delayed crack nucleation, energy dissipation, and the mechanism responsible for corresponding failure regime. The solvent osmolarity changes from ~400 mOsm in healthy joints to approximately ~250-300 mOsm in case of loss of proteoglycans, in rheumatoid osteoarthritis or in other diseased states (Sampat et al., 2013; Shanfield et al., 1988), so the findings from this study can help identify the influence of osmolarity (hyper-vs hypo-osmolarity) on the mechanical behavior of the cartilage and ultimately can aid in providing adequate medical treatment to the patients. The results of this study explain the holistic effect on the cartilage matrix behavior due to collagen fibril re-arrangement, altered permeability, and distribution of the charged biomacromolecules. Similar to previous studies showing enhanced fracture toughness of interpenetrating networks of agarose and poly(ethylene glycol) under modified single-notch edge test (Xiao et al., 2014), the importance of collagen fiber orientation and their density to the crack morphology and tissue mechanics (Moo et al., 2021a), differences in the mechanical behavior of the intact and crack mature and immature cartilage (Moo et al., 2021b), the findings in this study demonstrating effect of osmolarity and displacement rates thereby altering microstructural changes could be used to develop tissue engineering constructs and understand the failure mechanism of hydrogels, or of food-grade materials such as gelatin. The findings could be used to inform computational approaches by adding solvent based parameters including failure parameters, which would extend prior computational work (e.g. (Ebrahimi et al., 2019; Keenan et al., 2013; Meloni et al., 2017; Orozco et al., 2022; Taffetani et al., 2014),). These findings could also be used to guide replacement strategies by providing target failure properties. Overall, these findings provided new insight into the effects of osmolarity and displacement rate, and thereby PG/GAG concentration and collagen fiber configuration on fracture nucleation in articular cartilage. Additionally, these data provided evidence of two failure regimes in articular cartilage.

#### CRediT authorship contribution statement

**Dipul Chawla:** Visualization, Formal analysis, Data curation, Conceptualization, Investigation, Methodology, Software, Validation, Writing – original draft, Writing – review & editing. **Melih Eriten:** Visualization, Supervision, Resources, Funding acquisition, Conceptualization, Project administration, Writing – original draft, Writing – review & editing. **Corinne R. Henak:** Visualization, Supervision, Resources, Funding acquisition, Conceptualization, Project administration, Writing – original draft, Writing – review & editing.

#### **Declaration of competing interest**

The authors declare that they have no known competing financial interests or personal relationships that could have appeared to influence the work reported in this paper.

#### Data availability

Data will be made available on request.

#### Acknowledgements

Funding from the National Science Foundation (CMMI-DCSD-1662456), UW-Madison VCGRE, and the William F. Vilas Trust are gratefully acknowledged. Tissue from UW-Madison Meat Lab is gratefully acknowledged.

#### Appendix A. Supplementary data

Supplementary data to this article can be found online at https://doi.org/10.1016/j.jmbbm.2022.105467.

#### References

- Atkinson, T., Haut, R., Altiero, N., 1998. Impact-induced fissuring of articular cartilage: an investigation of failure criteria. J. Biomech. Eng. 120, 181–187.
- Bartell, L.R., Xu, M.C., Bonassar, L.J., Cohen, I., 2018. Local and global measurements show that damage initiation in articular cartilage is inhibited by the surface layer and has significant rate dependence. J. Biomech. 72, 63–70. https://doi.org/ 10.1016/j.jbiomech.2018.02.033.
- Bircher, K., Merluzzi, R., Wahlsten, A., Spiess, D., Simões-Wüst, A.P., Ochsenbein-Kölble, N., Zimmermann, R., Deprest, J., Mazza, E., 2020. Influence of osmolarity and hydration on the tear resistance of the human amniotic membrane. J. Biomech. 98 https://doi.org/10.1016/j.jbiomech.2019.109419.
- Bonifasi-Lista, C., Lake, S.P., Small, M.S., Weiss, J.A., 2005. Viscoelastic properties of the human medial collateral ligament under longitudinal, transverse and shear loading. J. Orthop. Res. 23, 67–76. https://doi.org/10.1016/j.orthres.2004.06.002.
- Briscoe, B.J., Sebastian, K.S., Adams, M.J., 1994. The effect of indenter geometry on the elastic response to indentation. J. Phys. D Appl. Phys. 27, 1156–1162. https://doi. org/10.1088/0022-3727/27/6/013.
- Chang, R., Kaplan, L.J., 1977. The Donnan equilibrium and osmotic pressure. J. Chem. Educ. 54, 218. https://doi.org/10.1021/ed054p218.
- Chawla, D., Han, G., Eriten, M., Henak, C.R., 2021. Microindentation technique to create localized cartilage microfractures. Curr. Protoc. https://doi.org/10.1002/cpz1.280.
- Chiravarambath, S., Simha, N.K., Namani, R., Lewis, J.L., 2009. Poroviscoelastic cartilage properties in the mouse from indentation. J. Biomech. Eng. 131, 011004 https://doi.org/10.1115/1.3005199.
- Cross, R., 1999. Standing, walking, running, and jumping on a force plate. Am. J. Phys. 67, 304–309. https://doi.org/10.1119/1.19253.
- Dempster, A.P., Laird, N.M., Rubin, D.B., 1977. Maximum likelihood from incomplete data via the EM algorithm. J. R. Stat. Soc. Ser. B 39, 1–22. https://doi.org/10.1111/j.2517-6161.1977.tb01600.x.
- Deneweth, J.M., Newman, K.E., Sylvia, S.M., McLean, S.G., Arruda, E.M., 2013. Heterogeneity of tibial plateau cartilage in response to a physiological compressive strain rate. J. Orthop. Res. 31, 370–375. https://doi.org/10.1002/jor.22226.
- Ebrahimi, M., Ojanen, S., Mohammadi, A., Finnilä, M.A., Joukainen, A., Kröger, H., Saarakkala, S., Korhonen, R.K., Tanska, P., 2019. Elastic, viscoelastic and fibrilreinforced poroelastic material properties of healthy and osteoarthritic human tibial cartilage. Ann. Biomed. Eng. 47, 953–966. https://doi.org/10.1007/s10439-019-02012-02
- Edelsten, L., Jeffrey, J.E., Burgin, L.V., Aspden, R.M., 2010. Viscoelastic deformation of articular cartilage during impact loading. Soft Matter 6, 5206–5212. https://doi.org/ 10.1039/c0sm00097c.
- Eisenberg, S.R., Grodzinsky, A.J., 1985. Swelling of articular cartilage and other connective tissues: Electromechanochemical forces. J. Orthop. Res. 3, 148–159. https://doi.org/10.1002/jor.1100030204.
- Han, E., Chen, S.S., Klisch, S.M., Sah, R.L., 2011. Contribution of proteoglycan osmotic swelling pressure to the compressive properties of articular cartilage. Biophys. J. 101, 916–924. https://doi.org/10.1016/j.bpj.2011.07.006.
- Han, G., Chowdhury, U., Eriten, M., Henak, C.R., 2021. Relaxation capacity of cartilage is a critical factor in rate- and integrity-dependent fracture. Sci. Rep. 11, 1–12. https://doi.org/10.1038/s41598-021-88942-w.
- Han, G., Eriten, M., Henak, C.R., 2019. Rate-dependent crack nucleation in cartilage under microindentation. J. Mech. Behav. Biomed. Mater. 96, 186–192. https://doi. org/10.1016/j.jmbbm.2019.04.015.
- Hardingham, T.E., Muir, H., Kwan, M.K., Lai, W.M., Mow, V.C., 1987. Viscoelastic properties of proteoglycan solutions with varying proportions present as aggregates. J. Orthop. Res. 5, 36–46. https://doi.org/10.1002/jor.1100050107.
- Henak, C.R., Bartell, L.R., Cohen, I., Bonassar, L.J., 2017. Multiscale strain as a predictor of impact-induced fissuring in articular cartilage. J. Biomech. Eng. 139 https://doi. org/10.1115/1.4034994.
- Huang, C.-Y., Soltz, M.A., Kopacz, M., Mow, V.C., Ateshian, G.A., 2003. Experimental verification of the roles of intrinsic matrix viscoelasticity and tension-compression nonlinearity in the biphasic response of cartilage. J. Biomech. Eng. 125, 84–93. https://doi.org/10.1115/1.1531656.
- Hwang, J.W., Chawla, D., Han, G., Eriten, M., Henak, C.R., 2022. Journal of the Mechanical Behavior of Biomedical Materials Effects of solvent osmolarity and

- viscosity on cartilage energy dissipation under high-frequency loading. J. Mech. Behav. Biomed. Mater. 126, 105014 https://doi.org/10.1016/j. imbbm.2021.105014.
- Jeffrey, J.E., Gregory, D.W., Aspden, R.M., 1995. Matrix damage and chondrocyte viability following a single impact load on articular cartilage. Arch. Biochem. Biophys. https://doi.org/10.1006/abbi.1995.1439.
- Kaleem, B., Maier, F., Drissi, H., Pierce, D.M., 2017. Low-energy impact of human cartilage: predictors for microcracking the network of collagen. Osteoarthritis Cartilage. https://doi.org/10.1016/j.joca.2016.11.009.
- Kaplan, J.T., Neu, C.P., Drissi, H., Emery, N.C., Pierce, D.M., 2017. Cyclic loading of human articular cartilage: the transition from compaction to fatigue. J. Mech. Behav. Biomed. Mater. 65, 734–742. https://doi.org/10.1016/j.jmbbm.2016.09.040.
- Keenan, K.E., Pal, S., Lindsey, D.P., Besier, T.F., Beaupre, G.S., 2013. A viscoelastic constitutive model can accurately represent entire creep indentation tests of human patella cartilage. J. Appl. Biomech. 29, 292–302. https://doi.org/10.1123/ iab.29.3.292.
- Khalsa, P.S., Eisenberg, S.R., 1997. Compressive behavior of articular cartilage is not completely explained by proteoglycan osmotic pressure. J. Biomech. 30, 589–594. https://doi.org/10.1016/S0021-9290(97)84508-3.
- Korhonen, R.K., Jurvelin, J.S., 2010. Compressive and tensile properties of articular cartilage in axial loading are modulated differently by osmotic environment. Med. Eng. Phys. 32, 155–160. https://doi.org/10.1016/j.medengphy.2009.11.004.
- Kujala, U.M., Kaprio, J., Sarno, S., 1994. Osteoarthritis of weight bearing joints of lower limbs in former elite male athletes. BMJ 308, 231. https://doi.org/10.1136/ bmj.308.6923.231.
- Lakes, P.R., 2009. Viscoelastic Materials, 1 edition. Cambridge University Press, Cambridge: New York.
- Lawless, B.M., Sadeghi, H., Temple, D.K., Dhaliwal, H., Espino, D.M., Hukins, D.W.L., 2017. Viscoelasticity of articular cartilage: Analysing the effect of induced stress and the restraint of bone in a dynamic environment. J. Mech. Behav. Biomed. Mater. 75, 293–301. https://doi.org/10.1016/j.jmbbm.2017.07.040.
- Levett, P.A., Hutmacher, D.W., Malda, J., Klein, T.J., 2014. Hyaluronic acid enhances the mechanical properties of tissue-engineered cartilage constructs. PLoS One 9. https://doi.org/10.1371/journal.pone.0113216.
- Lieberman, D.E., Venkadesan, M., Werbel, W.A., Daoud, A.I., Dandrea, S., Davis, I.S., Mangeni, R.O., Pitsiladis, Y., 2010. Foot strike patterns and collision forces in habitually barefoot versus shod runners. Nature 463, 531–535. https://doi.org/ 10.1038/nature08723.
- Liu, F., Kozanek, M., Hosseini, A., Van de Velde, S.K., Gill, T.J., Rubash, H.E., Li, G., 2010. In vivo tibiofemoral cartilage deformation during the stance phase of gait. J. Biomech. 43, 658–665. https://doi.org/10.1016/j.jbiomech.2009.10.028.
- Long, L.L., Srinivasan, M., 2013. Walking, running, and resting under time, distance, and average speed constraints: Optimality of walk-run-rest mixtures. J. R. Soc. Interface 10. https://doi.org/10.1098/rsif.2012.0980.
- Lu, X.L., Sun, D.D.N., Guo, X.E., Chen, F.H., Lai, W.M., Mow, V.C., 2004. Indentation determined mechanoelectrochemical properties and fixed charge density of articular cartilage. Ann. Biomed. Eng. 32, 370–379. https://doi.org/10.1023/B: ABME.0000017534.06921.24
- Mak, A.F., 1986. The apparent viscoelastic behavior of articular cartilage—the Contributions from the intrinsic matrix viscoelasticity and interstitial fluid Flows. J. Biomech. Eng. 108, 123–130. https://doi.org/10.1115/1.3138591.
- Maroudas, A., 1976. Balance between swelling pressure and collagen tension in normal and degenerate cartilage Growth of algal symbionts in regenerating hydra. Nature 260, 808–809.
- Maroudas, A., Wachtel, E., Grushko, G., Katz, E.P., Weinberg, P., 1991. The effect of osmotic and mechanical pressures on water partitioning in articular cartilage. Biochim. Biophys. Acta Gen. Subj. 1073, 285–294. https://doi.org/10.1016/0304-4165(91)00133-2
- Martin-Alarcon, L., Schmidt, T.A., 2016. Rheological effects of macromolecular interactions in synovial fluid. Biorheology 53, 49–67. https://doi.org/10.3233/BIR-15104
- Meloni, G.R., Fisher, M.B., Stoeckl, B.D., Dodge, G.R., Mauck, R.L., 2017. Biphasic finite element modeling Reconciles mechanical properties of tissue-engineered cartilage constructs across testing platforms. Tissue Eng. 23, 663–674. https://doi.org/ 10.1089/ten.tea.2016.0191.
- Moo, E.K., Al-Saffar, Y., Le, T., Seerattan, R.A., Pingguan-Murphy, B.K., Korhonen, R., Herzog, W., 2021a. Deformation behaviors and mechanical impairments of tissue cracks in immature and mature cartilages. J. Orthop. Res. https://doi.org/10.1002/ ior.25243
- Moo, E.K., Tanska, P., Federico, S., Al-Saffar, Y., Herzog, W., Korhonen, R.K., 2021b. Collagen fibres determine the crack morphology in articular cartilage. Acta Biomater. 126, 301–314. https://doi.org/10.1016/j.actbio.2021.03.031.
- Mora, J.C., Przkora, R., Cruz-Almeida, Y., 2018. Knee osteoarthritis: Pathophysiology and current treatment modalities. J. Pain Res. 11, 2189–2196. https://doi.org/ 10.2147/JPR.S154002.
- Moulinet, S., Adda-Bedia, M., 2015. Popping balloons: a case study of dynamical fragmentation. Phys. Rev. Lett. 115, 1–5. https://doi.org/10.1103/ PhysRevLett.115.184301.
- Mow, V.C., Kuei, S.C., Lai, W.M., Armstrong, C.G., 1980. Biphasic creep and stress relaxation of articular cartilage in compression: theory and experiments. J. Biomech. Eng. 102, 73. https://doi.org/10.1115/1.3138202.
- Mow, V.C., Ratcliffe, A., Robin Poole, A., 1992. Cartilage and diarthrodial joints as paradigms for hierarchical materials and structures. Biomaterials 13, 67–97. https:// doi.org/10.1016/0142-9612(92)90001-5.

- Mow, V.C., Wang, C.C., Hung, C.T., 1999. The extracellular matrix, interstitial fluid and ions as a mechanical signal transducer in articular cartilage. Osteoarthritis Cartilage 7, 41–58. https://doi.org/10.1053/joca.1998.0161.
- Myers, E.R., Lai, W.M., Mow, V.C., 1984. A continuum theory and an experiment for the ion-induced swelling behavior of articular cartilage. J. Biomech. Eng. 106, 151–158. https://doi.org/10.1115/1.3138473.
- Nalla, R.K., Kinney, J.H., Ritchie, R.O., 2003. Mechanistic fracture criteria for the failure of human cortical bone. Nat. Mater. 2, 164–168. https://doi.org/10.1038/nmat832.
- Nguyen, A.M., Levenston, M.E., 2012. Comparison of osmotic swelling influences on meniscal fibrocartilage and articular cartilage tissue mechanics in compression and shear. J. Orthop. Res. 30, 95–102. https://doi.org/10.1002/jor.21493.
- Nia, H.T., Bozchalooi, I.S., Li, Y., Han, L., Hung, H.H., Frank, E., Youcef-Toumi, K., Ortiz, C., Grodzinsky, A., 2013. High-Bandwidth AFM-based rheology reveals that cartilage is most sensitive to high loading rates at early stages of impairment. Biophys. J. 104, 1529–1537. https://doi.org/10.1016/j.bpj.2013.02.048.
- Nia, H.T., Han, L., Li, Y., Ortiz, C., Grodzinsky, A., 2011. Poroelasticity of cartilage at the nanoscale. Biophys. J. 101, 2304–2313. https://doi.org/10.1016/j.bpj.2011.09.011.
- Orozco, G.A., Tanska, P., Gustafsson, A., Korhonen, R.K., Isaksson, H., 2022. Crack propagation in articular cartilage under cyclic loading using cohesive finite element modeling. J. Mech. Behav. Biomed. Mater. 131, 105227 https://doi.org/10.1016/j. jmbbm.2022.105227.
- Peters, A.E., Comerford, E.J., Macaulay, S., Bates, K.T., Akhtar, R., 2017.
  Micromechanical properties of canine femoral articular cartilage following multiple freeze-thaw cycles. J. Mech. Behav. Biomed. Mater. 71, 114–121. https://doi.org/10.1016/j.jmbbm.2017.03.006.
- Puxkandl, R., Zizak, I., Paris, O., Keckes, J., Tesch, W., Bernstorff, S., Purslow, P., Fratzl, P., 2002. Viscoelastic properties of collagen: synchrotron radiation investigations and structural model. Philos. Trans. R. Soc. Lond. B Biol. Sci. 357, 191–197. https://doi.org/10.1098/rstb.2001.1033.
- Qu, C., Hirviniemi, M., Tiitu, V., Jurvelin, J.S., Töyräs, J., Lammi, M.J., 2014. Effects of freeze-thaw cycle with and without Proteolysis inhibitors and cryopreservant on the biochemical and biomechanical properties of articular cartilage. Cartilage 5, 97–106. https://doi.org/10.1177/1947603513515998.
- Repo, R.U., Finlay, J.B., 1977. Survival of articular cartilage after controlled impact. J. Bone Joint Surg. Am. 59, 1068–1076.
- Robinson, William H., Lepus, C.M., Wang, Q., Raghu, H., Mao, R., Lindstrom, T.M., Sokolove, J., 2016. Low-grade inflammation as a key mediator of the pathogenesis of osteoarthritis. Nat. Rev. Rheumatol. 12, 580–592. https://doi.org/10.1038/nrrheum.2016.136.
- Rodriguez, M.Z., Comin, C.H., Casanova, D., Bruno, O.M., Amancio, D.R., Costa, L. da F., Rodrigues, F.A., 2019. Clustering algorithms: a comparative approach. PLoS One 14, 1–34. https://doi.org/10.1371/journal.pone.0210236.
- Sadeghi, H., Lawless, B.M., Espino, D.M., Shepherd, D.E.T., 2018. Effect of frequency on crack growth in articular cartilage. J. Mech. Behav. Biomed. Mater. 77, 40–46. https://doi.org/10.1016/j.jmbbm.2017.08.036.
- Sadeghi, H., Shepherd, D.E.T., Espino, D.M., 2015. Effect of the variation of loading frequency on surface failure of bovine articular cartilage. Osteoarthritis Cartilage 23, 1–7. https://doi.org/10.1016/j.joca.2015.06.002.
- Sampat, S.R., Dermksian, M.V., Oungoulian, S.R., Winchester, R.J., Bulinski, J.C., Ateshian, G.A., Hung, C.T., 2013. Applied osmotic loading for promoting development of engineered cartilage. J. Biomech. 46, 2674–2681. https://doi.org/ 10.1016/j.jbiomech.2013.07.043.
- Shanfield, S., Campbell, P., Baumgarten, M., Bloebaum, R., Sarmiento, A., 1988. Synovial fluid osmolality in osteoarthritis and rheumatoid arthritis. Clin. Orthop. Relat. Res. 289–295. https://doi.org/10.1097/00003086-198810000-00029.
- Shergold, O.A., Fleck, N.A., 2005. Experimental investigation into the Deep penetration of soft solids by Sharp and Blunt Punches, with application to the piercing of Skin. J. Biomech. Eng. 127, 838. https://doi.org/10.1115/1.1992528.
- Silyn-Roberts, H., Broom, N.D., 1990. Fracture behavior of cartilage-on-bone in response to repeated impact loading. Connect. Tissue Res. 24, 143–156.
- Soulhat, J., Buschmann, M.D., Shirazi-Adl, A., 1999. A fibril-network-reinforced biphasic model of cartilage in unconfined compression. J. Biomech. Eng. 121, 340–347. https://doi.org/10.1115/1.2798330.
- Springhetti, R., Selyutina, N.S., 2018. Viscoelastic modeling of articular cartilage under impact loading. Meccanica 53, 519–530. https://doi.org/10.1007/s11012-017-0717-y.
- Taffetani, M., Griebel, M., Gastaldi, D., Klisch, S.M., Vena, P., 2014. Poroviscoelastic finite element model including continuous fiber distribution for the simulation of nanoindentation tests on articular cartilage. J. Mech. Behav. Biomed. Mater. 32, 17–30. https://doi.org/10.1016/j.jmbbm.2013.12.003.
- Tamer, T.M., 2013. Hyaluronan and synovial joint: function, distribution and healing. Interdiscipl. Toxicol. 6, 111–125. https://doi.org/10.2478/intox-2013-0019.
- Temple, D.K., Cederlund, A.A., Lawless, B.M., Aspden, R.M., Espino, D.M., 2016.
  Viscoelastic properties of human and bovine articular cartilage: a comparison of frequency-dependent trends. Submitt. BMC Musculoskelet. Disord. 1–8. https://doi.org/10.1186/s12891-016-1279-1.
- Torzilli, P.A., 1985. Influence of cartilage conformation on its equilibrium water partition. J. Orthop. Res. 3, 473–483. https://doi.org/10.1002/jor.1100030410.
- Torzilli, P.A., Grigiene, R., Borrelli, J., Helfet, D.L., 1999. Effect of impact load on articular cartilage: cell metabolism and viability, and matrix water content. J. Biomech. Eng. 121, 433–441.
- Trampel, R., Schiller, J., Naji, L., Stallmach, F., Kärger, J., Arnold, K., 2002. Self-diffusion of polymers in cartilage as studied by pulsed field gradient NMR. Biophys. Chem. 97, 251–260. https://doi.org/10.1016/S0301-4622(02)00078-9.

- Tran, D.T., Juang, Y.C., Tsai, L., 2021. Contrary response of porcine articular cartilage below and over 1000 s-1. Clin. Biomech. 90, 105506 https://doi.org/10.1016/j.clinbiomech.2021.105506.
- Urban, J.P.G., Maroudas, A., Bayliss, M.T., Dillon, J., 1979. Swelling pressures of proteoglycans at the concentrations found in cartilaginous tissues. Biorheology 16, 447–464. https://doi.org/10.3233/BIR-1979-16609.
- Vandenberghe, N., Villermaux, E., 2013. Geometry and fragmentation of soft brittle impacted bodies. Soft Matter 9, 8162–8176. https://doi.org/10.1039/c3sm50789k.
- Verteramo, A., Seedhom, B.B., 2007. Effect of a single impact loading on the structure and mechanical properties of articular cartilage. J. Biomech. 40, 3580–3589. https://doi.org/10.1016/j.jbiomech.2007.06.002.
- Vledouts, A., Vandenberghe, N., Villermaux, E., 2015. Fragmentation as an aggregation process. Proc. R. Soc. A Math. Phys. Eng. Sci. 471 https://doi.org/10.1098/ rsna 2015 1678
- Wachtel, E., Maroudas, A., 1998. The effects of pH and ionic strength on intrafibrillar hydration in articular cartilage. Biochim. Biophys. Acta Gen. Subj. 1381, 37–48. https://doi.org/10.1016/S0304-4165(97)00158-X.
- Xiao, Y., Rennerfeldt, D.A., Friis, E.A., Gehrke, S.H., Detamore, M.S., 2014. Evaluation of apparent fracture toughness of articular cartilage and hydrogels. J. Tissue Eng. Regen. Med. https://doi.org/10.1002/term.
- Zimmerman, B.K., Nims, R.J., Chen, A., Hung, C.T., Ateshian, G.A., 2021. Direct osmotic pressure measurements in articular cartilage demonstrate nonideal and concentration-dependent phenomena. J. Biomech. Eng. 143, 1–15. https://doi.org/ 10.1115/1.4049158.